Journal of Power Sources 212 (2012) 1–12

Contents lists available at SciVerse ScienceDirect

Journal of Power Sources

journal homepage: www.elsevier.com/locate/jpowsour

Synthesis of ordered mesoporous boron-containing carbon films and their corrosion behavior in simulated proton exchange membrane fuel cells environment

Tao Wang [a], ChuanXiang Zhang [b], Xin Sun [a], Yunxia Guo [a], Hu Guo [a], Jing Tang [a], Hairong Xue [a], Mingzhu Liu [a], Xiaoxue Zhang [a], Lei Zhu [a], Qiaoqiao Xie [a], Jianping He [a,*]

[a] College of Material Science and Technology, Nanjing University of Aeronautics and Astronautics, Yudao Street 29, 210016 Nanjing, PR China
[b] Research Laboratory of Hydrothermal Chemistry, Faculty of Science, Kochi University, 780-8520 Kochi, Japan

ARTICLE INFO

Article history:
Received 14 January 2012
Received in revised form
17 March 2012
Accepted 19 March 2012
Available online 11 April 2012

Keywords:
Bipolar plates
Boron-containing carbon films
Electrical conductivity
304 Stainless steel
Corrosion resistance

ABSTRACT

The ordered mesoporous boron-containing carbon films are deposited on 304 stainless steel (304 SS) as bipolar plate material for proton exchange membrane fuel cells (PEFMCs) by spin-coating method. As shown by XRD, N_2 adsorption–desorption and TEM, the composite films exhibit ordered mesoporous structures. The SEM and Raman results show that the carbon film is dense, continuous, and amorphous. The corrosion resistance, hydrophobicity and electrical conductivity, of the carbon-coated steel are investigated and compared to carbon-coated 304 SS. The ordered mesoporous boron-containing carbon film has high chemical inertness, thereby significantly enhancing the corrosion resistance of the coated 304 SS. Furthermore, the ordered mesoporous boron-containing carbon film is more hydrophobic and conductive than mesoporous carbon film. Therefore, the ordered mesoporous boron-containing carbon film-coated 304 stainless steel is a promising candidate for bipolar plate materials in PEMFCs.

1. Introduction

The bipolar plate is one of the most important components in proton exchange membrane fuel cells (PEMFCs) stacks and accounts for almost 80% of the total weight and 50% of the total cost [1–3]. The requirements of materials suitable for use as bipolar plates must be high electric conductivity, high corrosion resistance, sufficient mechanical integrity, low gas permeability and low-cost materials. More recent studies show that stainless steel may be a highly valuable material for metal bipolar plates, due to its many properties such as mechanical strength, electrochemical resistance, hardness, surface finish, cleanliness and neatness [4–7]. The main problem is that corrosion-resistant metal bipolar plates develop a passivating oxide layer on the surface that does protect the bulk metal from continuous corrosion, but also cause an undesirable effect of a high bulk contact resistance, especially as the passivating oxide layer is thickened during operation. Moreover, another problem associated with the use of stainless steel is corrosion or dissolution, in a weakly acidic medium usually containing SO_4^{2-}, Cl^-, F^- ions, etc. Then the dissolution of metals contaminates the entire membrane. The passivation and dissolution of metals during operation undoubtedly cause the dissipation of some electric energy and a reduction in the overall efficiency of the fuel cell power stack [8–10]. Therefore, varieties of coatings, such as carbon-based [11–15] and metal-based [16–19] coatings, have been investigated to protect the metallic bipolar plates from the corrosive operating conditions of fuel cell. Carbon film-coated stainless steel has been evaluated as a low-cost and small-volume substitute for graphite bipolar plate in PEMFCs. Many studies indicate that when a carbon-based layer is coated on the surface of metal bipolar plate whose passive film has been completely eliminated, the interfacial contact resistance could be reduced observably [12].

Hence, various carbonaceous materials, such as graphite, conductive polymer, diamond-like carbon, and organic self-assembled monopolymers, used as carbon-based coatings of bipolar plates, have been investigated widely [20–22]. Fukutsuka indicated that carbon-coating on stainless steel (SUS304) carried out by plasma-assisted CVD [12] showed a high electric conductivity compared with uncoate SUS304. Though there was not the passive film between the carbon-coating and SUS304, the dynamic polarization behavior of carbon-coated SUS304 under PEMFC

* Corresponding author. Tel./fax: +86 25 52112626.
E-mail address: jianph@nuaa.edu.cn (J. He).

0378-7753/$ – see front matter © 2012 Elsevier B.V. All rights reserved.
doi:10.1016/j.jpowsour.2012.03.068

operating conditions improved. Chung *et al.* [13] systematicly analyzed the corrosion behavior of carbon film-coated 304 stainless steels as PEMFCs bipolar plates, and found that the carbon film revealed excellent chemical stability similar to that of the high-purity graphite plate, which successfully protected 304 stainless steels substrate against the corrosive environment in PEMFCs. Feng *et al.* [15,23] reported that carbon films which are dense, continuous, and amorphous, were deposited on stainless steel 316L samples by close field unbalanced magnetron sputtering, and better than those of conventional graphite bipolar plates. The deposited carbon film was more hydrophobic and had high chemical inertness. Its interfacial contact resistance was elevated to that of graphite. Thereby, the carbon films significantly enhanced the corrosion resistance of the coated stainless steel 316L.

A new approach is coating a mesoporous carbon-based film on the stainless steel substrate by spin-coating method. The carbon-based composite film showed an optimal corrosion resistance, with extremely stable potentiostatic polarization process in the simulated fuel cells environment [21]. Although mesoporous carbon-based films have many advantages such as excellent corrosion resistance, further improvement including electrical conductivity is needed for them to meet the applications. Many researches on carbon materials have shown that modification with electron-donating or electron-withdrawing elements, such as N, P, and B, could change the electronic properties of carbons and produce additional functional groups on the carbon surface [24–28].

Hence, in order to improve the electrical conductivity of mesoporous C-based film [21], Wang *et al.* synthesized conductive polyaniline films on mesoporous C-based film by potentiostatic method, and then the polyaniline/mesoporous C-based films were pyrolyzed at low temperatures under N_2 atmosphere to obtain nitrogen-containing C-based films [29]. The whole process is extremely tedious and high-cost, and the N modifying process belongs to post-treatment of the preformed mesoporous materials. In most cases of ordered mesoporous carbons, the modified process of incorporate heteroatoms is accomplished by post-treatment, which is simple but less controllable in either the amount or distribution of dopants. The modified process may also bring about partial or even complete destruction of the ordered mesoporous structure, which is undesirable in applications [30,31].

In this paper, we expect to directly incorporate heteroatoms into the carbon precursors before carbonization, which may get a homogeneous distribution of heteroatoms, while maintain the ordered mesoporous structure. In order to improve the electrical conductivity and high dehydration of mesoporous carbon film on substrates of 304 stainless steels, ordered boron-containing carbon (CB) films were synthesized by using resols as an organic precursor, boric acid as a heteroatom precursor, and amphiphilic triblock copolymer F127 as a template, with evaporation-induced tricon-stituent co-assembly method. Ordered mesoporous CB film is used for the first time in this study as corrosion protective coating on 304 stainless steels. Characterization of the morphology, structure and physical properties of these ordered mesoporous CB films and protective properties against corrosion exposed to sulfuric acid solution to simulate PEMFCs environment have been elucidated in detail.

2. Experimental

2.1. Chemicals

Triblock copolymer Pluronic F127 ($M_w = 12{,}600$, $EO_{106}PO_{70}EO_{106}$) was purchased from Sigma–Aldrich Corp. Boric acid, phenol, formalin solution (37 wt%), NaOH, HCl, H_2SO_4 and ethanol were purchased from Shanghai Chemical Corp. All chemicals were used as received without any further purification. Millipore water was used in all experiments. The low-molecular-weight resol (phenol-formaldehyde, $M_w < 500$) as a carbon source was prepared according to the procedure reported by the Zhao group [32].

2.2. Synthesis of mesoporous boron-containing carbon films

In a typical synthesis of ordered mesoporous CB film, 1.0 g of triblock copolymer Pluronic F127 and 1.8 mL of 0.6 mol L^{-1} HCl were poured into 20.0 mL of ethanol with vigorous stirring to obtain a clear solution. To this solution, a certain amount of boric acid (0.02 g, 0.04 g, 0.08 g, 0.16 g) and 5 g of resol (20 wt% in ethanol) were added in succession. After stirring for 2 h, a homogeneous solution was obtained. The film was fabricated by spin-coating the solution onto clean type 304 stainless steel at 1500 rpm for 60 s using an SPINCOATER KW-4A, the same process was repeated for 5 times. The film was aged at room temperature for 12 h and then thermopolymerized in an oven at 100 °C for 24 h. The result brown deposit was carbonized in a tubular furnace at 350 °C for 5 h, and then at 400, 500, 600 or 700 °C for 2 h respectively, under N_2 atmosphere using always a heating rate of 1 °C min^{-1}. Ordered boron-doped carbon film was obtained and denoted as CB-*x*-*y*, where *x* represented the mass ratio of boric acid to resol, *y* represents the carbonized temperature. When the *x* is 0, the mesoporous film is named CB-0, that is ordered mesoporous carbon film without boron. The ordered mesoporous films with different compositions in a wide range from 0 to 3.6% of boric acid to resol were prepared by varying the content of boric acid.

2.3. Characterization

The powder X-ray diffraction (XRD) patterns were obtained using a Bruker D8 Advance diffractometer using a Cu Ka source (λ = 0.154056 nm) at 40 kV and 40 mA. Raman spectra were obtained with a french JY HR800 microscopic Raman system, using a He–Ne laser at an excitation wavelength of 633 nm. Nitrogen adsorption–desorption isotherms were measured at 77 K using a Micromeritics ASAP 2010 instrument. Surface areas of the samples were calculated using the BET (Brunauer–Emmett–Teller) equation, while the pore size distributions were determined by the BJH (Barret–Hoyner–Halenda) method using the adsorption branch. The structural characteristics of samples were investigated by FT-IR spectroscopy in the range 4000–400 cm^{-1} using a Nicolet NEXUS-670 and KBr pellets of solid samples. Water contact angles were measured by a contact angle system SL200B (SOLON. Tech., China). The in-plane electrical conductivity was measured by the Wentworth Laboratories 6514 System Electrometer Keithley. Transmission electron microscopy (TEM) experiments and selected area electron diffraction (SAED) pattern were conducted by a FEI Tecnai G^2 system operated at 200 kV. The samples for TEM measurements were suspended in ethanol and supported on a holey carbon film on a Cu grid. Energy dispersive X-ray spectrum (EDS) installed in FEI Tecnai G^2 system was also used to analyze the microzone composition of the sample. The field emission scanning electron microscopy (FE-SEM) images were recorded on a Hitachi S-4800 microscope with an accelerating voltage of 15 kV, to observe the surface of the films. Thermogravimetric (TG) measurements of the products were monitored using a NETZSCH-STA 409 PC from 30 to 800 °C under air with a heating rate of 10 °C min^{-1}.

2.4. Electrochemical measurements

All electrochemical experiments were carried out in 0.5 mol L^{-1} H_2SO_4 aqueous solution using a standard three-electrode cell with

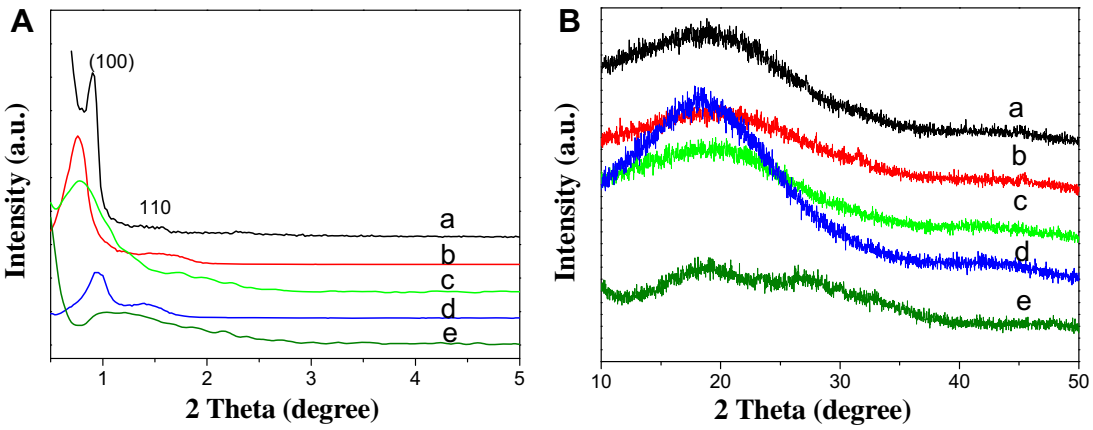

Fig. 1. (A) Small-angle XRD and (B) Wide-angle XRD patterns of ordered mesoporous CB films: (a) CB-0%-500, (b) CB-0.45%-500, (c) CB-0.9%-500, (d) CB-1.8%-500 and (e) CB-3.6%-500.

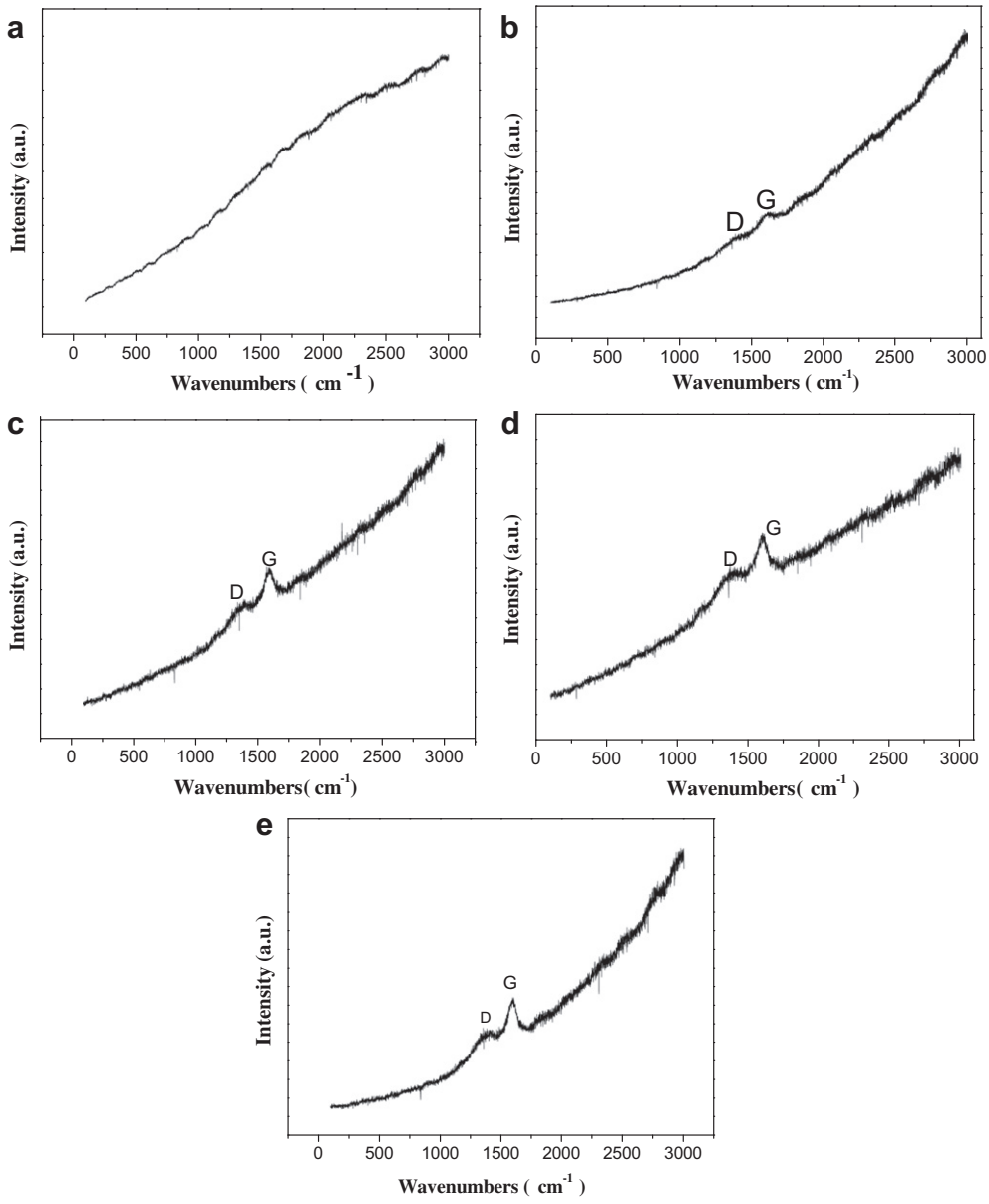

Fig. 2. Raman spectra of ordered mesoporous CB films: (a) CB-0%-500, (b) CB-0.45%-500, (c) CB-0.9%-500, (d) CB-1.8%-500 and (e) CB-3.6%-500.

Table 1
The values of contact angles with water and electrical conductivity for 304 SS and the mesoporous CB films.

Sample	Contact angle (°)	Surface energy (N m^{-2})	G (S m^{-1})
304 SS	60.73	40.4	–
CB-0-500	71.00	32.0	0.0043
CB-0.45%-500	72.95	30.4	0.0056
CB-0.9%-500	78.04	26.5	0.067
CB-1.8%-500	79.56	25.4	0.089
CB-3.6%-500	86.12	20.8	0.15

a coated or uncoated 304 SS sheet as working electrode, an SCE as reference electrode, and a platinum foil as counter electrode. For all working electrodes a corrosion surface area of 1 cm^2 has been considered. Due to the fact that each working electrode has been coated only on one side, the uncoated face and the edges have been protected from the acid solution with an epoxy resin. The film electrodes were stabilized in the solution at open circuit for 60 min. An electrochemical interface (Solartron 1287) was employed to conduct potentiodynamic polarization measurements at a scan rate of 10 mV s^{-1}. Potentiostatic polarizations were conducted on a Solartron 1287, to investigate the performance and stability of the films, the polarizations were recorded at applied anode potential of −100 mV (SCE) and cathode potential +600 mV (SCE) for PEMFCs. Potentiostatic polarizations were conducted at room temperature and 80 °C. Electrochemical impedance spectroscopy (EIS) measurements using Solartron 1260 frequency response analyzer coupled to Solartron 1287 potentiostat were obtained at frequencies between 100 kHz and 0.01 Hz. The amplitude of the sinusoidal potential signal was 5 mV.

3. Results and discussion

3.1. Ordered mesoporous boron-containing carbon film—effect of the boron content

3.1.1. Characterization of ordered mesoporous boron-containing carbon film

To investigate the effect of boron content on the ordered mesoporous structure, graphitization degree, and corrosion resistance of the mesoporous carbon-based film, different amounts of boron source were used in the self-assembly process. Energy dispersive X-ray spectrum (EDS) (Fig. S1) of ordered mesoporous CB film is offered in the "Supplementary content", and we can find that boron has been introduced into the framework of the amorphous ordered mesoporous carbon. The small-angle XRD patterns of the samples are shown in Fig. 1(A). An intense Bragg diffraction peak and a weak peak were observed at around $2\theta = 1°$ and 1.5°, respectively, indicating an ordered 2D hexagonal mesoporous structure. However, when the boron content reached 3.6%, the reflection of (100) became weak, suggesting that a high content of boron, would induce a deterioration of the long-range structural order [29,33].

The graphitic structure of the obtained CB films is further confirmed by wide-angle XRD pattern and Raman spectra. As shown in Fig. 1(B), the wide-angle XRD patterns of mesoporous CB films heated at 500 °C reveals a broad diffraction peak at around $2\theta = 19°$, which attributed to the amorphous carbon. However, when boron was incorporated excessively, the resulting CB-3.6%-500 shows a weak peak at around $2\theta = 28°$, indicating that a small quantity of hydrogen borate exists (reference code 00-030-0620), and a weak peak at around $2\theta = 23°$, indicating that a small quantity of semi-graphitized carbon exists. With boron incorporated into the carbon framework, the degree of graphitization is enhanced by the effect of catalytic graphitization [34–37].

Raman spectra of ordered mesoporous CB films are given in Fig. 2. A distinct pair of broad bands at 1600 cm^{-1} (G band) and 1380 cm^{-1} (D band) can be observed, after carbon films are doped with boron. The D band of the samples shows a very weak hump at around 1380 cm^{-1}, which can be assigned to vibration of sp^3-hybridized carbon atoms in a disordered carbon structure [38]. The G band is due to vibration of sp^2-hybridized carbon atoms in the graphite layer, which means the carbon–carbon stretching (E2g) mode of the hexagonal graphite [39]. Therefore, the relative intensities of the I_D/I_G reflect graphitization degree of carbon films, the smaller I_D/I_G, the higher graphitization degree. For doped boron carbon films, both the D and G bands become sharp and the intensity increases with the increase of boron content, compared to mesoporous CB-0-500, suggesting an improvement of order within the graphene layers [40,41]. This result indicates a change from amorphous carbon to nanocrystalline graphite or graphite-like carbon with enhanced degree of graphitization.

In addition, surface property and electrical conductivity of bipolar plates are important influences of cell performances. When the PEMFCs are operating, the liquid water is continually generated due to oxygen reduction reaction. If the liquid water could not be

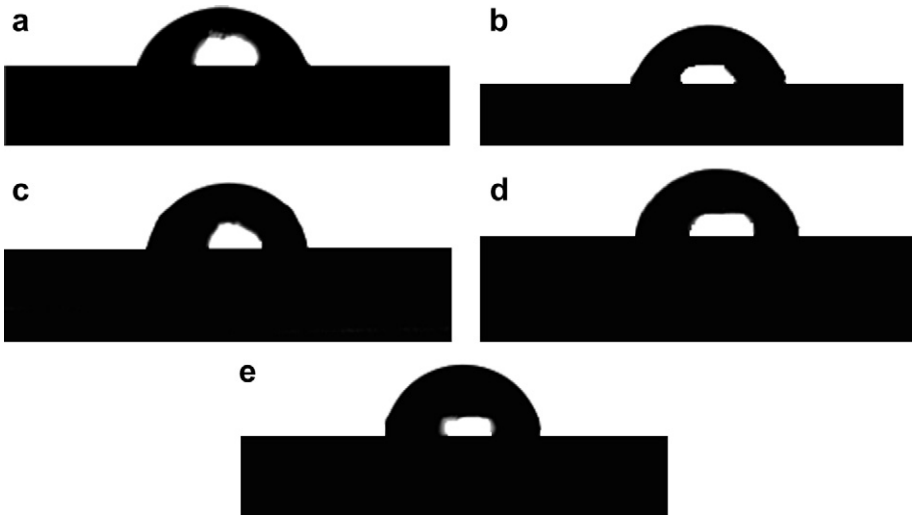

Fig. 3. The contact angle of ordered mesoporous CB films: (a) CB-0%-500, (b) CB-0.45%-500, (c) CB-0.9%-500, (d) CB-1.8%-500 and (e) CB-3.6%-500.

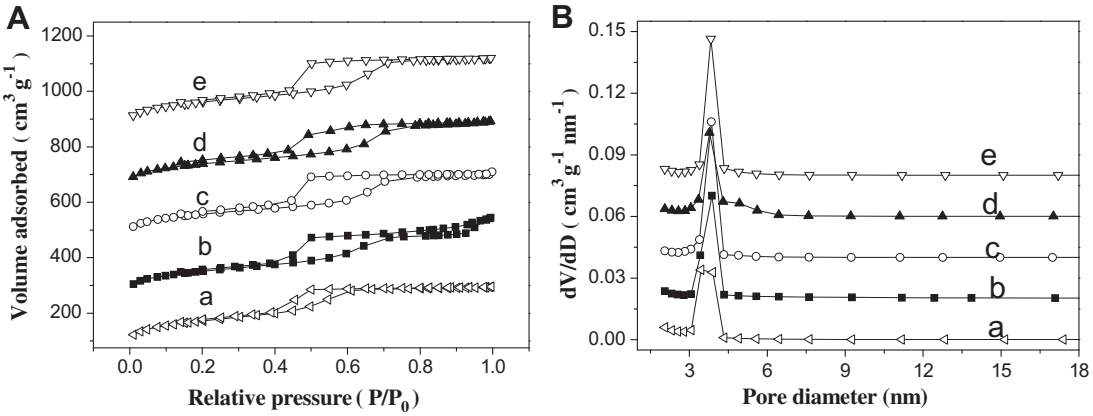

Fig. 4. N_2 adsorption–desorption isotherm (A) and pore size distribution (B) of ordered mesoporous CB films: (a) CB-0%-500, (b) CB-0.45%-500, (c) CB-0.9%-500, (d) CB-1.8%-500 and (e) CB-3.6%-500. For clarity, the isotherms (A) for the CB-0.45%-500, CB-0.9%-500, CB-1.8%-500 and CB-3.6%-500 are offset vertically by 200, 400, 600, 800 $cm^3\ g^{-1}$, respectively. The isotherms (B) for the CB-0.45%-500, CB-0.9%-500, CB-1.8%-500, CB-3.6%-500 are offset vertically by 0.02, 0.04, 0.06, 0.08 $cm^3\ g^{-1}\ nm^{-1}$, respectively.

removed in time, the water would block the reactant gases access to the electrode and even induce the flooding phenomenon. So, the bipolar plates materials that are suitable for transportation applications should have a lower value of surface property and a water contact angle close to 90° [9]. In the progress of the carbonization, those hydrophilic groups of the films, such as oxygen-containing functional groups, would transfer to small molecules which would volatilize. Therefore, with the increase of the graphitization, the surface of the carbon film will consist of nonpolar graphitic carbon, and then the carbon film has the worse wettability. On the other hand, the electrical conductivity of carbon material is also proportional to the graphitic degree of carbon material. Therefore, surface property and the electrical conductivity measurements are conducted to demonstrate the graphitization degree of the carbon films and the results are collected in Table 1. The contact angles of the samples with water are shown in Fig. 3. The contact angle value of the uncoated 304 SS is approximately 60–70°. Water is produced during the operation of the PEMFCs. The water will flood, if the generation rate of liquid water at the cathode exceeds the removal rate from the cathode. The bipolar plate should be hydrophobic, because the contact angle increases with improvement in the hydrophobic property. The large contact angle of stainless steel with coatings favors water removal to prevent accumulated water from flooding the electrode system. Jin *et al.* reported that a carbon film was deposited on 304 SS using close field unbalanced magnetron sputter ion plating and had a much larger average contact angle of 88.6°, while the average contact angle value of the uncoated 304 SS is 67.4° [42]. A molybdenum nitride diffusion coating has been prepared on the surface of AISI 304 304 SS by plasma surface diffusion alloying method, the molybdenum nitride diffusion coating increases the contact angle of the 304 SS from 68 to 91°, which indicates that the MoeN 304 SS is more hydrophobic than the untreated one [43]. Pulsed bias arc ion plating was used to form Cr-nitride films on stainless steel, the coated sample has a bigger contact angle (95°) than uncoated stainless steel (73°) [44].

Table 2
Structural parameters of CB-x-500 films.

Sample	$S_{BET}/m^2\ g^{-1}$	$V_{total}/cm^3\ g^{-1}$	$R_{meso}/\%$	D/nm
CB-0%-500	588	0.46	76.1%	3.1
CB-0.45%-500	518	0.53	83.0%	4.1
CB-0.9%-500	533	0.48	79.2%	3.6
CB-1.8%-500	475	0.45	84.5%	3.8
CB-3.6%-500	551	0.50	80.0%	3.6

A closed field unbalanced magnetron sputter ion plating method was used by Yi *et al.* to deposit amorphous carbon (a-C) film on 304 SS bipolar plates as an alternative to protect the materials against the corrosive electrolyte of PEMFCs [45]. The contact angle of a-C coated 304 SS is 78.8° while that of bare 304 SS is 73.2°. These results demonstrate that the surface energy of a-C coated 304 SS is improved by the a-C coating. We can know from Table 1 that CB-3.6%-500 owns the highest water contact angle and electrical conductivity, suggesting that boron possesses the effect of catalytic graphitization and promote the graphitic degree of carbon film, which is in accord with the results of wide-angle XRD patterns and Raman spectra. The test data indicates that the ordered mesoporous CB-*x* films are more hydrophilic than 304 SS and the ordered mesoporous carbon film that is CB-0, and so the CB-*x* film with a higher water contact angle would be helpful for water removal in the stack and be beneficial to the simplification of water management. The electrical conductivity for these films is shown in Table 1. It shows that the ordered mesoporous C–B films have bigger water contact angle and electrical conductivity than mesoporous pure carbon film without boron (CB-0), consistent with the results of wide-angle XRD patterns and Raman spectra.

Fig. 4 illustrates the N_2 adsorption–desorption isotherms of ordered mesoporous CB-500 films, and corresponding pore size distribution curves obtained from the adsorption branch. The

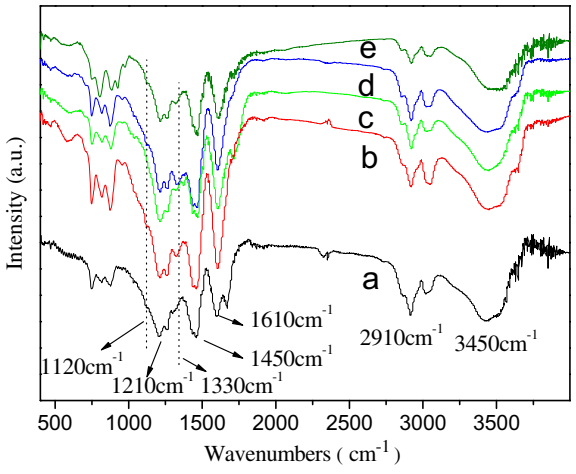

Fig. 5. FT-IR spectra of ordered mesoporous CB films: (a) CB-0%-500, (b) CB-0.45%-500, (c) CB-0.9%-500, (d) CB-1.8%-500 and (e) CB-3.6%-500.

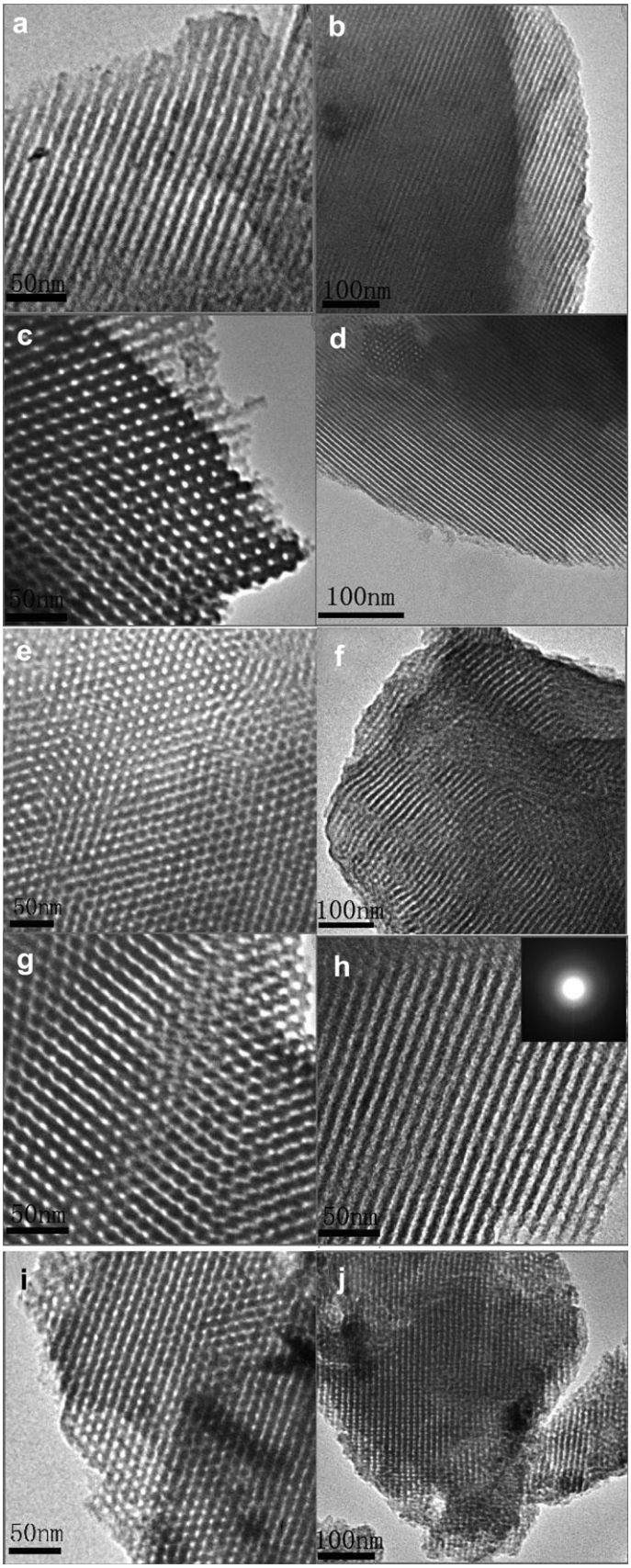

Fig. 6. TEM images of ordered mesoporous CB films: (a,b) CB-0-500, (c,d) CB-0.02-500, (e,f) CB-0.04-500, (g,h) CB-0.08-500 and (i,j) CB-0.16-500, viewed from the [001] (a, c, e, f, i) and [110] (b, d, f, h, j) directions. The inset in (h) is the SAED pattern of CB-0.08-500.

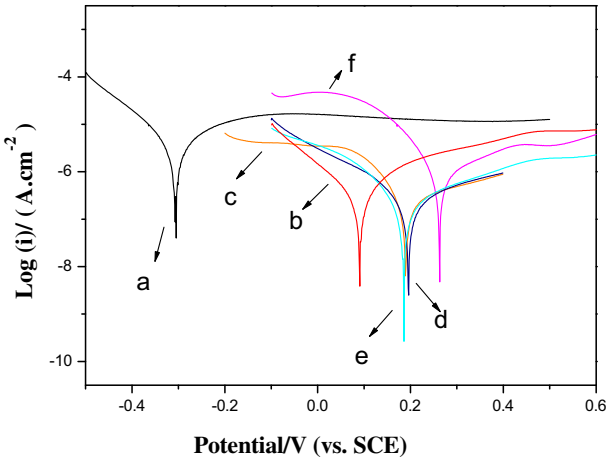

Fig. 7. Potentiodynamic polarization curves of ordered mesoporous CB film-coated and the bare 304 SS in 0.5 mol L^{-1} H_2SO_4 solution: (a) 304 SS, (b) CB-0%-500, (c) CB-0.45%-500, (d) CB-0.9%-500, (e) CB-1.8%-500 and (f) CB-3.6%-500.

Table 3
The corrosion current density (I_{corr}) and the corrosion potentials (E_{corr}) values for the mesoporous composite films in 0.5 M H_2SO_4.

Sample	E_{corr} (mV)(SCE)	I_{corr}/(μA cm^{-2})
304 SS	−305	5.36
CB-0-500	91	0.464
CB-0.45%-500	189	0.461
CB-0.9%-500	194	0.329
CB-1.8%-500	183	0.285
CB-3.6%-500	177	2.47

Brunauer–Emmett–Teller (BET) method was utilized to calculate the specific surface areas (S_{BET}) using adsorption data in a relative pressure range from 0.04 to 0.2. By using the Barrett–Joyner–Halenda (BJH) model, the pore volumes and pore size distributions were derived from the adsorption branches of isotherms, and the total pore volumes (V_{total}) were estimated from the adsorbed amount at a relative pressure P/P_0 of 0.992. Only one narrow peak is observed with the most probable distribution at 3.1–4.1 nm. The structural parameters of the films, including the BET surface area (S_{BET}), average pore size (D) and total pore volume (V_{total}) are presented in Table 2. All above mesoporous CB films have typical IV curve with a hysteresis loop in the middle relative pressure range suggests a narrow mesopore size distribution.

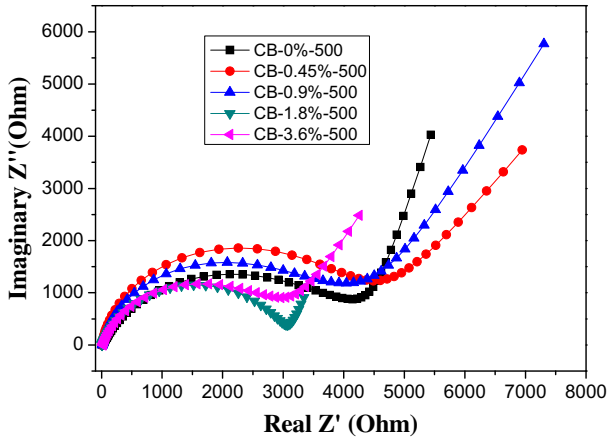

Fig. 9. Electrochemical impedance spectra of ordered mesoporous CB films-coated 304 SS in 0.5 mol L^{-1} H_2SO_4 solution.

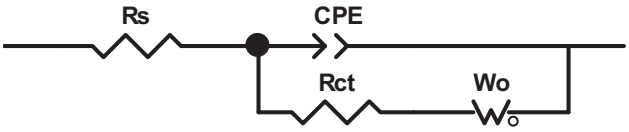

Fig. 10. Equivalent circuit representing the corrosion of the ordered mesoporous CB films-coated 304 SS in 0.5 mol L^{-1} H_2SO_4 solution.

The FT-IR spectra (Fig. 5) of the ordered mesoporous CB films samples show five intense bands at 1210 cm^{-1}, 1450 cm^{-1}, 1610 cm^{-1}, 2910 cm^{-1}, and 3450 cm^{-1}. The peaks at about 1210 cm^{-1} and 2910 cm^{-1} are duo to the C–O and C–H stretching [46,47]. The peak at about 1610 cm^{-1} can be assigned to the C=C double bond of the benzene ring, whereas the peak at 1450 cm^{-1} is due to the bending of the C–H bond [46,47]. For all samples, the characteristic peaks at around 3450 cm^{-1} can be attributed to the stretching vibration of the –OH group of adsorbed water molecules. There is a weak peak at about 1120 cm^{-1}, which may come from the stretching vibration of the B–O band. The peak at 1330 cm^{-1} can be attributed to the stretching vibration of C–B [48].

A more detailed structural characterization is revealed by TEM images, as shown in Fig. 6. These images viewed along the [001] and [110] directions, further confirm an ordered 2D hexagonal mesoporous structure, consistent with the results from the small-angle XRD (Fig. 1A) patterns. Characterized by wide-angle XRD (Fig. 1B) and the SAED pattern (Fig. 6h), we estimate that the walls

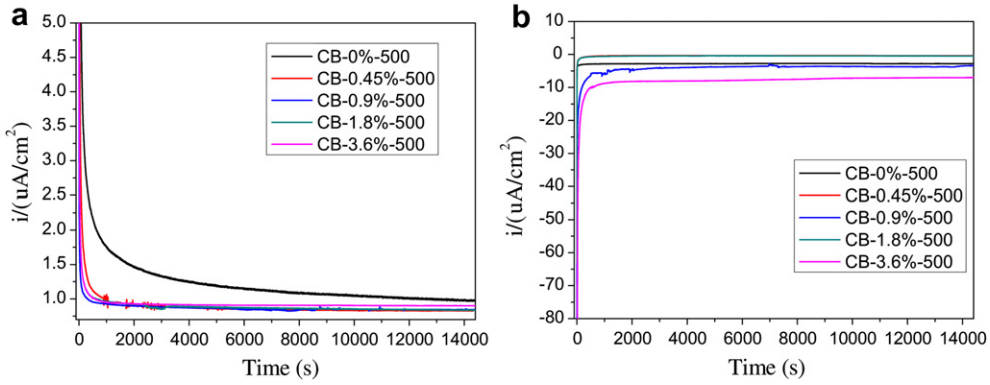

Fig. 8. Potentiostatic polarization curve of CB-0%-500, CB-0.45%-500, CB-0.9%-500, CB-1.8%-500, and CB-3.6%-500 at 600 mV (SCE) (a) and −100 mV (SCE) (b) In 0.5 mol L^{-1} H_2SO_4 solution.

Table 4
Fitted results of electrochemical impedance spectras.

Sample	R_s (Ω cm^2)	CPE (μF cm^{-2})	R_{ct} (Ω cm^2)	W_0-T
CB-0-500	21.2	130	3802	0.4154
CB-0.45%-500	6.5	180	3512	0.3054
CB-0.9%-500	15.6	109	3087	0.2710
CB-1.8%-500	7.5	298	3032	0.4025
CB-3.6%-500	26.0	45	2640	0.3449

of these mesoporous films are amorphous at calcination temperature of 500 °C. The TG curves show that the ordered mesoporous carbon films are thermally stable slightly over 350 °C as shown in Fig. S2. Moreover, ordered mesoporous boron-containing carbon film is more stable than the ordered mesoporous carbon film prepared without boric acid. It is possible to suggest the following explanation: (i) the effect of chemically bonded boric acid with phenolic resin inside the pore wall, and (ii) the role of C—B bond to enhance the thermal stability which was formed during the heating treatment process in the N_2.

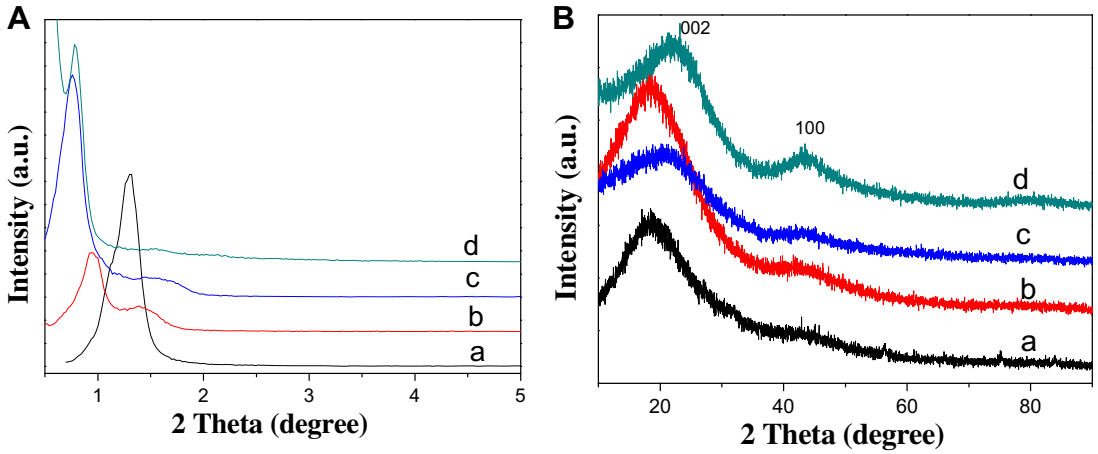

Fig. 11. (A) Small-angle XRD and (B) Wide-angle XRD patterns of ordered mesoporous CB films: (a) CB-1.8%-400, (b) CB-1.8%-500, (c) CB-1.8%-600, and (d) CB-1.8%-700.

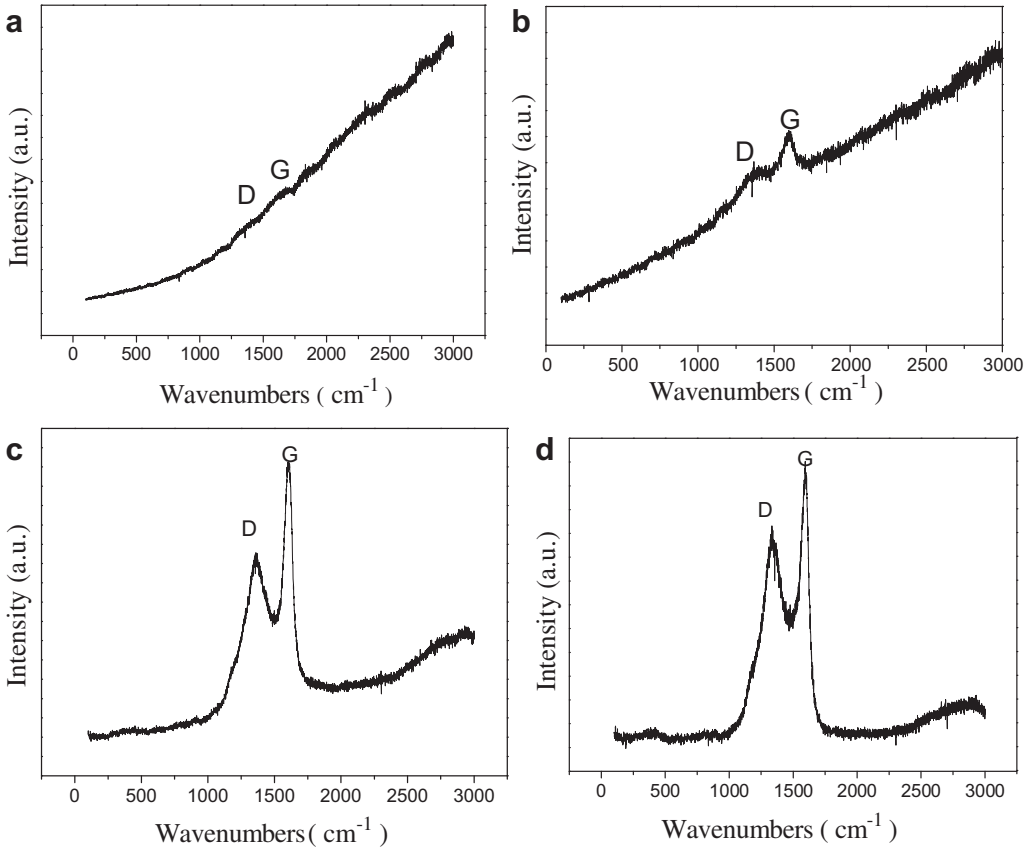

Fig. 12. Raman spectra of ordered mesoporous CB films: (a) CB-1.8%-400, (b) CB-1.8%-500, (c) CB-1.8%-600, and (d) CB-1.8%-700.

Table 5
The values of contact angles with water and electrical conductivity for the mesoporous CB films.

Sample	Contact angle (°)	Surface energy (N m^{-2})	G (S m^{-1})
CB-1.8%-400	65.68	36.3	0.0085
CB-1.8%-500	79.56	25.4	0.089
CB-1.8%-600	82.05	23.6	1.78
CB-1.8%-700	84.66	21.8	2.96

3.1.2. Electrochemical polarization measurements of ordered mesoporous boron-containing carbon film

Fig. 7 shows the potentiodynamic polarization curves for uncoated and for the mesoporous film-coated 304 SS after immersion in 0.5 mol L^{-1} H_2SO_4 aqueous solution for 1 h. The mesoporous film-coated 304 SS was found to induce a shift in the corrosion potential to a more positive value, as would be expected, since the film acts as a physical barrier to corrosion [49]. The corrosion potential and corrosion current determined by potentiodynamic polarization extrapolations for these films are shown in Table 3. E_{corr} and the corrosion current density (I_{corr}) for 304 SS are −305 mV (SCE) and 5.36 μA cm^{-2} respectively, while E_{corr} increases for the ordered mesoporous carbon film-coated steel (CB-0) by about 390 mV (SCE) and I_{corr} is lower than that for the bare steel by 1 orders of magnitude. It is evident that the corrosion resistance of 304 SS significantly increases with mesoporous film coating in 0.5 mol L^{-1} H_2SO_4 solution. When we introduce the boron in mesoporous carbon, the E_{corr} increases for the ordered mesoporous CB film-coated steel by about 90 mV (SCE) and I_{corr} is lower than that for the mesoporous carbon by 1 order of magnitude. Wherein, CB-1.8%-500 displays the larger corrosion potential and lowest corrosion current, signifying good corrosion resistance. We think that the introduction of boron with appropriate contents, may increase the contact angles with water, and not destroy the ordered mesoporous structure, and even enhance the stability with a perfect compact structure. When the content of boric acid reaches to 3.6%, the ordered mesoporous structure has been disrupted, and correspondingly the corrosion current is observably bigger than other mesoporous film.

Fig. 8(a) shows the potentiostatic polarization curve for the ordered mesoporous CB film-coated steel in 0.5 mol L^{-1} H_2SO_4 solution at +600 mV (SCE). The polarization current of CB-0%-500 decreased slowly with time to the level of 1.1 μA cm^{-2}. However, the polarization current of CB-x-500 ($x = 0.45–3.6\%$) film decreased instantly with time to the level of 0.8 μA cm^{-2}, significantly lower than the passive current for the CB-0%-500 film. Besides, the CB-x-500 films are quite stable during the polarization, as is evidenced by the absence of the current density fluctuation, suggesting no degradation is observed after potentiostatic measurements and indicating the composite films are very stable at the cathode working potential of PEMFC. It is clear that all CB-x-500 films inhibit effectively the corrosion of the substrate steel. Fig. 8(b) shows the potentiostatic polarization curve of the ordered mesoporous CB film-coated 304 stainless steel in 0.5 mol L^{-1} H_2SO_4 solution at −100 mV (SCE). The polarization current density of CB-1.8%-500 film decreased significantly to a steady value of around −0.48 μA cm^{-2}. No degradation was observed after potentiostatic measurements for 4 h, indicating the high stability of CB-x-500 film at the anode working potential of PEMFC.

3.1.3. Electrochemical impedance measurements

Fig. 9 presents the electrochemical impedance spectra of the ordered mesoporous CB films-coated 304 SS in 0.5 mol L^{-1} H_2SO_4. The corresponding equivalent circuit is proposed to fit the impedance plots as seen in Fig. 10. R_s is the solution resistance, R_{ct} is the charge-transfer resistance, and the constant phase element (CPE) is accounted for the adsorptive double-layer capacitance of non-homogeneity interface. W_0 is the diffusion impedance and W_0-T is the Warburg coefficient. The fitting parameters using Zview—impedance analysis software 2.80 are shown in Table 4. From the electrochemical impedance spectra data for the ordered mesoporous CB films-coated 304 SS, we can see that the electrochemical impedance values of the mesoporous films-coated samples decrease with the increase of boron content. We believe there is a relationship between the electrochemical impedance values and the electron conductivity. All of the ordered mesoporous CB films show large semi-arc-shaped radius and a low W_0-T coefficient, indicating that their impedance in the electrochemical corrosion process is big, and that the diffusion process of corrosion products is slow. Therefore, they exhibit a high stability in H_2SO_4 solution, and are effective barriers to the inward penetration of test solution, thus, reduce significantly the corrosion of the substrate alloy.

3.2. Ordered mesoporous boron-containing carbon film—effect of the calcination tempertures

3.2.1. Characterization of ordered mesoporous boron-containing carbon film

To investigate the effect of calcination temperature on the structural order, graphitization degree, and protection performance of the resulting mesoporous thin films, different calcination temperatures were used in the heat treating process. As shown in Fig. 11(A), the results imply that the mesostructures are thermally stable and the hexagonal mesophases can be retained. The graphitic change with the increase of temperature of the obtained CB film is further confirmed by wide-angle XRD pattern and Raman

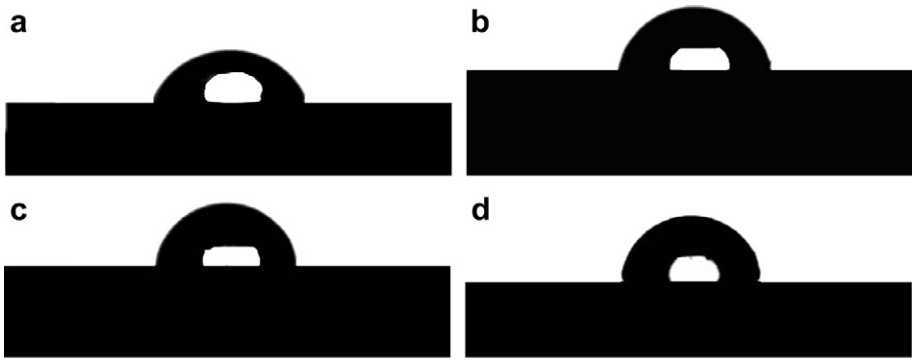

Fig. 13. The contact angle of ordered mesoporous CB films: (a) CB-1.8%-400, (b) CB-1.8%-500, (c) CB-1.8%-600, and (d) CB-1.8%-700.

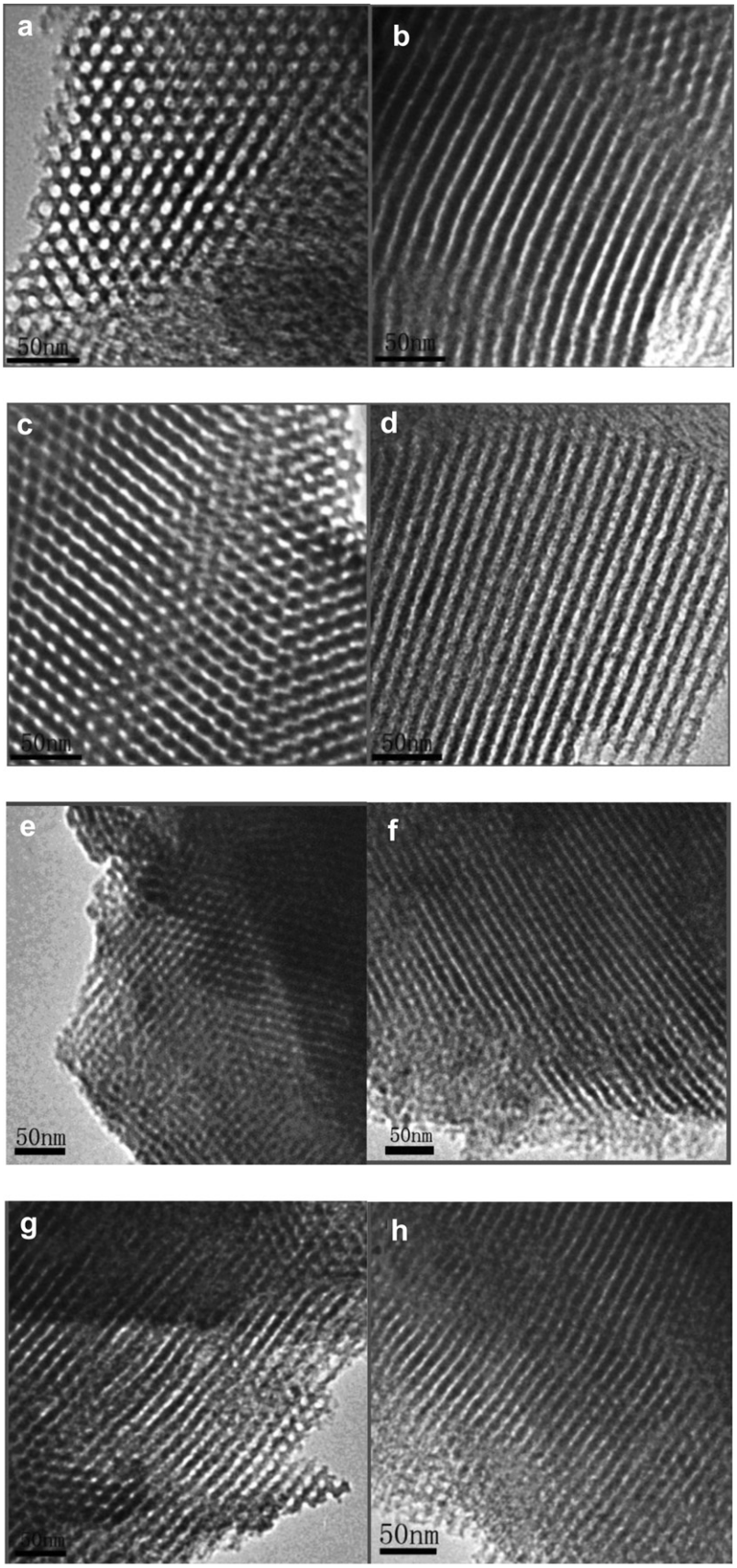

Fig. 14. TEM images of ordered mesoporous CB films: (a, b) CB-1.8%-400, (c, d) CB-1.8%-500, (e, f) CB-1.8%-600, and (g, h) CB-1.8%-700.

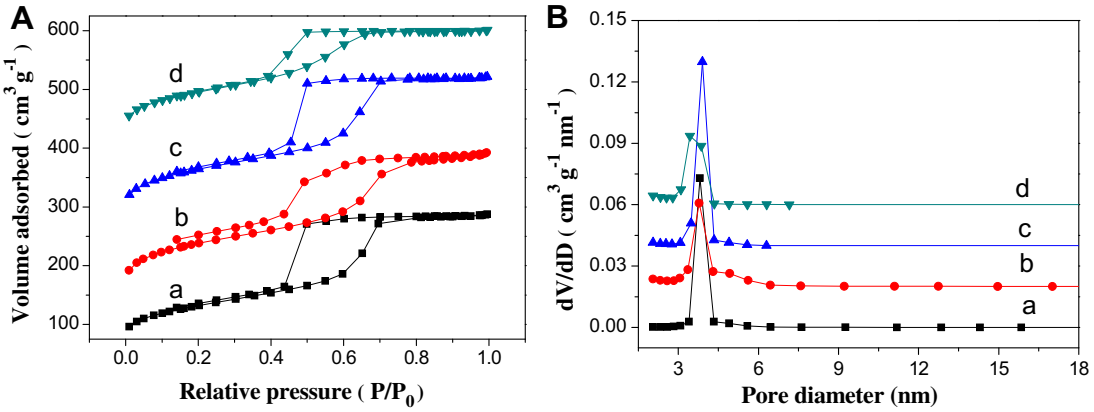

Fig. 15. N_2 adsorption–desorption isotherm (A) and pore size distribution(B) of ordered mesoporous CB films: of ordered mesoporous CB films: (a) CB-1.8%-400, (b) CB-1.8%-500, (c) CB-1.8%-600, and (d) CB-1.8%-700.

spectra. The wide-angle XRD patterns of mesoporous CB films heated at 400 and 500 °C reveals a broad diffraction peak at around $2\theta = 19°$, which is attributed to the amorphous carbon. After heated at 600 °C, two broad diffraction peaks at $2\theta = 22$ and 43°, which correspond to (002) and (101) diffractions of typical graphite-like carbon phase [50], were observed in the wide-angle XRD pattern of CB film (Fig. 11B). The results indicate that the prepared materials are graphitized during carbonization at 600 °C which is much lower than graphitized temperature of pure ordered mesoporous carbon [51]. The lower graphitized temperature of boron-containing carbon is due to the existence of the boron, which can accelerate the development of graphitic structure of carbon [52,53].

Raman spectra (Fig. 12) of ordered mesoporous CB-1.8% films calcined at different temperatures are given in Fig. 8. A distinct pair of broad bands at 1600 cm^{-1} (G band) and 1380 cm^{-1} (D band) can be observed, after carbon films are doped with boron calcined at 600 °C, suggesting an improvement of graphitic structure. This result also corresponds to a change from amorphous to nanocrystalline graphite or an enhanced degree of graphitization on the proposed amorphization trajectory.

Therefore, surface property and the electrical conductivity are collected in Table 5. The contact angles of the samples are shown in Fig. 13. We can know from Table 1 that CB-1.8%-700 owns the highest water contact angle and electrical conductivity, suggesting that the increase of calcination temperature promotes the graphitic degree of carbon film. These contact angle and electrical conductivity data are well in agreement with the wide-angle XRD (Fig. 11) and Raman spectra (Fig. 12) results.

The mesostructures of the CB films are investigated with TEM. As shown in Fig. 14, these images viewed along the [001] and [110] directions, further confirm an ordered 2D hexagonal mesoporous structure, which is consistent with the XRD results. Fig. 15 shows N_2 adsorption–desorption isotherms and pore size distribution of the four CB films, and Table 6 lists the corresponding textural parameters. All of the CB films exhibit typical type IV isotherms with an obvious H1-type hysteresis loop, indicating the mesoporous structures of the materials. The pore size distributions are very narrow, centering at around 3.6–3.9 nm for CB-1.8%-400, CB-1.8%-500 and CB-1.8%-600 (Fig. 6B). However, the samples with higher calcination temperature (700 °C) have a decreased pore size. Obviously, the mesoporous structure would shrink sharply at 700 °C, which may destroy the compactness of the film to affect its corrosion resistance. Fig. S3 shows SEM images of the CB-1.8%-500 film and CB-1.8%-700 film, the mesoporous film is composed of many 1-dimensional channels parallel to the substrate. Sure enough, we find that there are some cracks in the CB-1.8%-700 film, as shown in Fig. S3(c).

3.2.2. Electrochemical polarization measurements of ordered mesoporous boron-containing carbon film

Fig. 16 presents the potentiodynamic polarization curves for ordered mesoporous CB film-coated and the bare 304 SS in 0.5 mol L^{-1} H_2SO_4 aqueous solution at room temperature. The

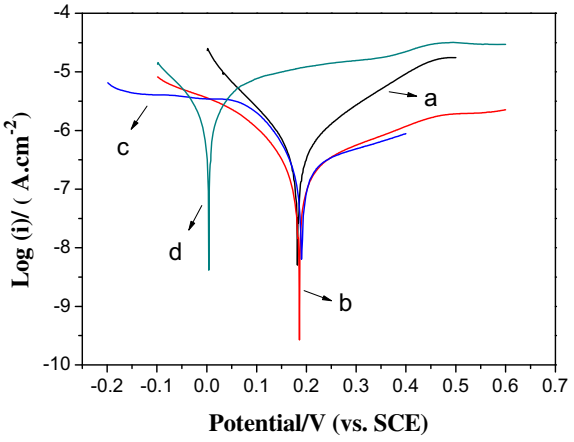

Fig. 16. Potentiodynamic polarization curves of ordered mesoporous CB film-coated and the bare 304 SS in 0.5 mol L^{-1} H_2SO_4 solution: (a) CB-1.8%-400, (b) CB-1.8%-500, (c) CB-1.8%-600, and (d) CB-1.8%-700.

Table 6
Structural parameters of CB-1.8%-y films.

Sample	S_{BET}/m^2 g^{-1}	V_{total}/cm^3 g^{-1}	R_{meso}/%	D/nm
CB-1.8%-400	451	0.44	81.8%	3.9
CB-1.8%-500	475	0.45	84.5%	3.8
CB-1.8%-600	555	0.50	78.0%	3.6
CB-1.8%-700	652	0.47	83.0%	2.9

Table 7
The corrosion current density (I_{corr}) and the corrosion potentials (E_{corr}) values for the mesoporous composite films in 0.5 M H_2SO_4.

Sample	E_{corr} (mV)(SCE)	I_{corr}/(μA cm^{-2})
CB-1.8%-400	182	0.583
CB-1.8%-500	189	0.285
CB-1.8%-600	190	0.601
CB-1.8%-700	4	3.73

corrosion potential and corrosion current determined by potentiodynamic polarization extrapolations for these films are shown in Table 7. It shows that the ordered mesoporous CB film has a larger corrosion potential and a low corrosion current, when the calcined temperature is under 700 °C, which means a good corrosion resistance. However, the CB-1.8% film which shrinks greatly at 700 °C, has a close corrosion current with the uncoated 304 SS. We think the low density of the CB film would reduce its corrosion resistance.

4. Conclusions

Boron was successfully introduced into an amorphous ordered mesoporous carbon by way of an experimental design utilizing an appropriate temperature range. By changing the amount of boric acid in the mixed solution we were able to change the amount of boron in the film. The introduction of boron can increase the graphitization of the samples under the same reaction conditions (time, temperature). Therefore, the described design allowed us to produce boron-doped carbon materials with higher graphitization than pure ordered mesoporous carbon at same calcined temperatures. We also believe that this method could be used to prepare other element-containing carbon film, such as N, P, S, F. These composite films exhibited excellent protective performance in 0.5 M H_2SO_4 corrosion system with a positive corrosion potential and a lower corrosion current. Wherein, the CB-1.8%-500 film shows the optimal protective performance, corresponding corrosion potential and corrosion current density are 183 mV and 0.285 $\mu A\ cm^{-2}$. We believe that the ordered mesoporous boron-containing carbon films have a potential application as a protect coating of bipolar plate material.

Acknowledgment

The authors appreciate the financial supports of the National Natural Science Foundation of China (50871053).

Appendix A. Supplementary material

Supplementary material associated with this article can be found, in the online version, at doi:10.1016/j.jpowsour.2012.03.068.

References

[1] I. Bar-On, R. Kirchain, R. Roth, J. Power Sources 109 (2002) 71–75.
[2] R. Kaiser, H.G. Fritz, C.D. Eisenbach, Proceedings of the 18th Stuttgarter Kunststoff–Kolloquium, Sprint Druck, Stuttgart, 2003, 3–4.
[3] H. Tsuchiya, O. Kobayashi, Int. J. Hydrogen Energy 10 (2004) 985–990.
[4] T.M. Wena, K.H. Hou, C.Y. Bai, M.D. Ger, P.H. Chien, S.J. Lee, Corros. Sci. 52 (2010) 3599–3608.
[5] R.F. Silva, D. Franchi, A. Leone, L. Pilloni, A. Masci, A. Pozio, Electrochim. Acta 51 (2006) 3592–3598.
[6] Y.J. Ren, C.L. Zeng, J. Power Sources 182 (2008) 524–530.
[7] Y.J. Ren, J. Chen, C.L. Zeng, J. Power Sources 195 (2010) 1914–1919.
[8] J. Wind, R. Späh, W. Kaiser, G. Böhm, J. Power Sources 105 (2002) 256–260.
[9] H. Tawfik, Y. Hung, D. Mahajan, J. Power Sources 163 (2007) 755–767.
[10] R.A. Antunes, M.C.L. Oliveira, G. Ett, V. Ett, Int. J. Hydrogen Energy 35 (2010) 3632–3647.
[11] S. Joseph, J.C. McClure, R. Chianelli, P. Pich, P.J. Sebastian, Int. J. Hydrogen Energy 30 (2005) 1339–1344.
[12] T. Fukutsuka, T. Yamaguchi, S.I. Miyano, Y. Matsuo, Y. Sugie, Z. Ogumi, J. Power Sources 174 (2007) 199–205.
[13] C.Y. Chung, S.K. Chen, P.J. Chiu, M.H. Chang, T.T. Hung, T.H. Ko, J. Power Sources 176 (2008) 276–281.
[14] Y. Fu, G.Q. Lin, M. Hou, B. Wu, Z. Shao, B. Yi, Int. J. Hydrogen Energy 34 (2009) 405–409.
[15] K. Feng, Y. Shen, H. Sun, D. Liu, Q. An, X. Cai, P.K. Chu, Int. J. Hydrogen Energy 16 (2009) 6771–6777.
[16] E.A. Cho, U.S. Jeon, S.A. Hong, I.H. Oh, S.G. Kang, J. Power Sources 142 (2005) 177–183.
[17] S.T. Myung, M. Kumagai, R. Asaishi, Y.K. Soon, H. Yashiro, Electrochem. Commun. 3 (2008) 480–484.
[18] E. Dur, Ö.N. Cora, M. Koç, Int. J. Hydrogen Energy 36 (2011) 7162–7173.
[19] H.B. Zhang, G.Q. Lin, M. Hou, L. Hu, Z.Y. Han, Y. Fu, Z.G. Shao, B.L. Yi, J. Power Sources 198 (2012) 176–181.
[20] A. Hermann, T. Chaudhuri, P. Spagnol, Int. J. Hydrogen Energy 30 (2005) 1297–1302.
[21] T. Wang, J.P. He, D. Sun, J.H. Zhou, Y.X. Guo, X.C. Ding, S.C. Wu, J.Q. Zhao, J. Tang, Corros. Sci. 53 (2011) 1498–1504.
[22] S. Kitta, H. Uchida, M. Watanabe, Electrochim. Acta 4 (2007) 2025–2033.
[23] K. Feng, X. Cai, H.L. Sun, Z.G. Li, P.K. Chu, Diamond Relat. Mater. 19 (2010) 1354–1361.
[24] R.L. Liu, D.Q. Wu, X.L. Feng, K. Müllen, Angew. Chem. Int. Ed. 49 (2010) 2565–2569.
[25] D. Hulicova-Jurcakova, M. Kodama, S. Shiraishi, H. Hatori, Z.H. Zhu, G.Q. Lu, Adv. Funct. Mater. 19 (2009) 1800–1809.
[26] J. Zhang, X. Liu, R. Blume, A. Zhang, R. Schlogl, D.S. Su, Science 322 (2008) 73–77.
[27] Y. Li, J. Zhong, X.Z. Yang, G.J. Lan, H.D. Tang, H.Z. Liu, New Carbon Mater. 26 (2011) 123–129.
[28] B.F. Abramovic, L.J. Bjelica, F.F. Gaal, V.J. Guzsvany, L.S. Jovanovic, Electroanalysis 15 (2003) 878–884.
[29] T. Wang, J.P. He, D. Sun, Y.X. Guo, Y.O. Ma, Y. Hu, G.X. Li, H.R. Xue, J. Tang, X. Sun, J. Power Sources 196 (2011) 9552–9560.
[30] M.B. Martin-Hopkins, R.K. Gilpin, M. Jaroniec, J. Chromatogr. Sci. 29 (1991) 147–158.
[31] J.L. Bahr, J.M. Tour, J. Mater. Chem. 12 (2002) 1952–1958.
[32] Y. Meng, D. Gu, F.Q. Zhang, Y.F. Shi, H.F. Yang, Z. Li, C.Z. Yu, B. Tu, D.Y. Zhao, Angew. Chem. Int. Ed. 44 (2005) 7053–7059.
[33] X.C. Zhao, A.Q. Wang, J.W. Yan, G.Q. Sun, L.X. Sun, T. Zhang, Chem. Mater. 22 (2010) 5463–5473.
[34] T. Sogabe, K. Nakajima, M. Inagaki, J. Mater. Sci. 31 (1996) 6469–6476.
[35] A. ŌYA, R. Yamashita, S. Ōtani, Fuel 58 (1979) 495–500.
[36] A. ŌYA, S. Ōtani, Carbon 17 (1979) 131–137.
[37] A. ŌYA, H. Marsh, J. Mater. Sci. 17 (1982) 309–322.
[38] P.K. Chu, L. Li, Mater. Chem. Phys. 96 (2006) 253–277.
[39] A.C.Y. Liu, R. Arenal, X.D. Chen, Phys. Rev. B 61 (2000) 14095.
[40] H.K. Jeong, Y.P. Lee, R.J.W.E. Lahaye, M.H. Park, K.H. An, I.J. Kim, C.W. Yang, C.Y. Park, R.S. Ruoff, Y.H. Lee, J. Am. Chem. Soc. 130 (2008) 1362–1366.
[41] I. Calizo, A.A. Balandin, W. Bao, F. Miao, C.N. Lau, Nano Lett. 7 (2007) 2645–2649.
[42] W.H. Jin, K. Feng, Z.G. Li, X. Cai, L. Yu, D.H. Zhou, J. Power Sources 196 (2011) 10032–10037.
[43] L.X. Wang, J.C. Sun, P.B. Li, J. Sun, Y. Lv, B. Jing, S. Li, S.J. Ji, Z.S. Wen, Int. J. Hydrogen Energy 37 (2012) 5876–5883.
[44] Y. Fu, G.Q. Lin, M. Hou, B. Wu, H.K. Li, L.X. Hao, Z.G. Shao, B.L. Yi, Int. J. Hydrogen Energy 34 (2009) 453–458.
[45] P.Y. Yi, L.F. Peng, L.Z. Feng, P. Gan, X.M. Lai, J. Power Sources 195 (2010) 7061–7066.
[46] Y.J. Kim, M.I.I. Kim, C.H. Yun, J.Y. Chang, C.R. Park, M. Inagaki, J. Colloid Interface Sci. 274 (2004) 555–562.
[47] K.A. Trick, T.E. Saliba, Carbon 33 (1995) 1509–1515.
[48] M.K. Lei, L.J. Yuan, Z.L. Zhang, T.C. Ma, J. Inorg. Mater. 14 (1999) 189–192.
[49] Y.B. Lee, C.H. Lee, D.S. Lim, Int. J. Hydrogen Energy 34 (2009) 9781–9787.
[50] M. Sevilla, A.B. Fuertes, Carbon 44 (2006) 468–474.
[51] X.Q. Wang, C.D. Liang, S. Dai, Langmuir 24 (2008) 7500–7505.
[52] T. Hamada, K. Suzuki, T. Kohno, T. Sugiura, Carbon 40 (2002) 1203–1210.
[53] J.S. Burgess, C.K. Acharya, J. Lizarazo, N. Yancey, B. Flowers, G. Kwon, T. Klein, M. Weaver, A.M. Lane, C.H. Turner, S. Street, Carbon 46 (2008) 1711–1717.